Supporting Information

Mechanisms of directional polymer crystallization

Alejandro A. Krauskopf[†], Andrew M. Jimenez[†], Elizabeth A. Lewis[ǁ], Bryan D. Vogt[§], Alejandro J. Müller[⊥‡], Sanat K. Kumar[†*]

[†]Department of Chemical Engineering, Columbia University, New York, New York 10027, United States

[ǁ]Department of Polymer Engineering, University of Akron, Akron, Ohio 44325, United States

[§]Department of Chemical Engineering, The Pennsylvania State University, University Park, Pennsylvania 16803, United States

[‡] POLYMAT and Department of Polymer Science and Technology, Faculty of Chemistry, Basque Country University UPV/EHU, Paseo Lardizabal 3, 20018, Donostia-San Sebastián, Spain.

[⊥] Ikerbasque, Basque Science Foundation, 48011, Bilbao, Spain

*Correspondence to sk2794@columbia.edu

Experimental methods

Materials and sample preparation

Poly(ethylene oxide) (PEO) was purchased from Scientific Polymer Products ($M_w = 100$ kg/mol, polydispersity $M_w/M_n = 4$). Tetrahydrofuran (THF) was purchased from Sigma-Aldrich (ACS reagent, ≥99.0%, contains 250 ppm BHT as inhibitor). Irganox 1010, an antioxidant, was donated by BASF and was added to PEO to mitigate thermal degradation.

PEO, along with 0.5 wt % Irganox, was dissolved and stirred in THF at 65 °C for 1 h. The solutions were then probe sonicated for 3 min using a 2 s on, 1 s off loop, then air dried in Teflon dishes inside a fume hood for 1 day. The samples were then annealed in a vacuum oven for 1 day at 80 °C, after which they were hot pressed at 80 °C into 100 μm-thick rectangular films with dimensions ≈ 8 mm x 50 mm for zone annealing and small disks for isothermal crystallization in the DSC.

Zone Annealing (ZA)

The peak temperature was generated by a current (BK Precision 1692 Switching Digital DC Power Supply) in circuit with a 0.064" diameter nickel chromium alloy wire (McMaster-Carr) encased in a 0.156" outer diameter ceramic tubing (McMaster-Carr). The temperature gradient is established by sandwiching the ceramic tubing with two cold plates (McMaster Carr) that are connected to a chiller system circulating water held at 15 °C. A thermal IR imaging camera (Testo 875i-1 Adjustable Focus Thermal Imager) was used to characterize the temperature gradient. The sample holder consists of a 50 mm x 75 mm x 1 mm glass slide lined on the borders with 1/16" thick silicone rubber strips, and another glass slide of the same dimensions placed on top of the rubber. The sample chamber was then sealed by wrapping the outer edges of the slides with Kapton tape. The sample holder was used to zone anneal two samples at a time. A motorized stage (Thorlabs KMTS50E) was translated at a set ZA velocity using the Thorlabs Kinesis software. Prior to translating the motorized stage, the temperature gradient established by the setup was allowed to equilibrate for 15 min. Jimenez et al.[1] have shown that holding 100 kg/mol PEO at 90 °C for 5 minutes is sufficient to remove thermal history from the sample. The fastest zone annealing velocity we probed was still slow enough that the amount of time any given portion of the sample (that undergoes melting and crystallization) stays between 90 °C and 115 °C is not less than 5 minutes.

Small-Angle X-ray Scattering (SAXS)

SAXS for the ZA samples was performed at Columbia University with a GANESHA by SAXSLAB laboratory scale scattering instrument with a Cu-Kα source (λ = 1.504 Å) and a Pilatus 300K detector. A q-range of 0.007-0.15 Å^{-1} was used for our measurements. $I(q)$ data was obtained by integrating the 2D scattering patterns using the pyFAI Python package.[2]

Differential Scanning Calorimetry (DSC)

Heat flow measurements were performed with a TA Instruments Discovery DSC calibrated for heat capacity with a sapphire disk and for temperature and enthalpy with indium. After ZA, the samples were cut into smaller rectangles of ≈5 mg and crimped in a standard aluminum DSC pan. The samples were subjected to a nonisothermal heating protocol from room temperature to 105 °C at a ramp rate of 10 °C/min under a nitrogen atmosphere.

The isothermal crystallizations were done according to the procedure by Jimenez et al.[1] Briefly, samples were ramped from room temperature to 90 °C at 20 °C/min and held at that temperature for 5 minutes to remove thermal history, after which they were ramped down to the desired T_c at 60 °C/min to avoid crystallization at temperatures other than T_c. The samples were held at T_c for at least $3 * t_{peak}$ (peak heat flow time during crystallization). The enthalpy of fusion, ΔH_f, was determined by ramping the samples to 90 °C at 10 °C/min and integrating under the resulting heat flow curve.

The crystal weight fraction, $\varphi_{c,w}$, was obtained by normalizing ΔH_f by 205.4 J/g, the enthalpy for 100% crystalline PEO.[3] The crystal volume fraction then follows the relation[4] $\varphi_{c,v} = \frac{\varphi_{c,w}}{\varphi_{c,w}+(\rho_c/\rho_a)(1-\varphi_{c,w})}$, where $\rho_c = 1.239$ g/cm^3 and $\rho_a = 1.1210$ g/cm^3 are the densities for crystalline[5] and amorphous[6] PEO, respectively.

Cross-Polarized Optical Microscopy (CPOM)

Micrographs were taken with a Nikon Eclipse Ti-U inverted microscope equipped with a Nikon DS-Ri2 camera.

Lauritzen-Hoffman Analysis

Isothermal spherulitic growth rate data at different temperatures were reported by Jimenez et al.[1] using a similar CPOM setup as our study. A linear fit to the data plotted as $ln(G)$ vs. $\frac{1}{T_c f \Delta T}$ allows for determination of the unknown parameters in the Lauritzen-Hoffman equation:[7] $G = G_0 \exp\left(-\frac{U^*}{R(T_c - T_\infty)}\right) \exp\left(-\frac{K_g}{T_c f \Delta T}\right)$, where all parameters were defined in the main text. T_c, f, and ΔT are all dependent on the crystallization temperature and as such vary during fitting; U^* is commonly treated as a constant in the literature,[8,9] and R, G_0, T_m^0, and $T_\infty = T_g - 30$ are constant values. The linear fit therefore allows us to solve for K_g; this fitting procedure is sensitive to the selected constant parameters, so these must be chosen appropriately.

Treatment of SAXS data and correlation function analysis

After wedge integration of 25° centered on the angle of maximum intensity, contributions from thermal density fluctuations are subtracted from these data by performing a nonlinear least squares fit to Porod's law for pinhole collimation, $I(q) = \frac{K_p}{q^4} + I_{th}$, where K_p is the Porod constant and I_{th} is the scattering intensity contribution from thermal density fluctuations.

The correlation function for each scattering profile is calculated according to Strobl and Schneider:[10]

$$G(r) = \frac{1}{2\pi^2} \int_0^\infty q^2 I(q) \cos(qr)\, dq \qquad (1)$$

where q is the scattering vector, $I(q)$ is the intensity at q, and r is the correlation distance. The calculation of the correlation function typically requires extrapolation of the intensity data to $q = 0$ and $q \to \infty$. Through our analysis, it was found that only the invariant was affected significantly by incorporating the extrapolated data into the integral; the parameters studied here were not shifted appreciably. However, for completeness, the extrapolation to both extremes is performed – see Figure S1. Porod's law for pinhole collimation is used for extrapolation to high q, with $I_{th} = 0$ as this correction has already been made. Extrapolation to $q = 0$ is done by a nonlinear least squares fit of the intensity data at low q to the Debye-Bueche relation for two-phase systems, $I(q) = \frac{I_0}{(1+(qa_0)^2)^2}$, where I_0 is the intensity at $q = 0$, and a_0 is a measure of the length scale of inhomogeneities in the system.[11]

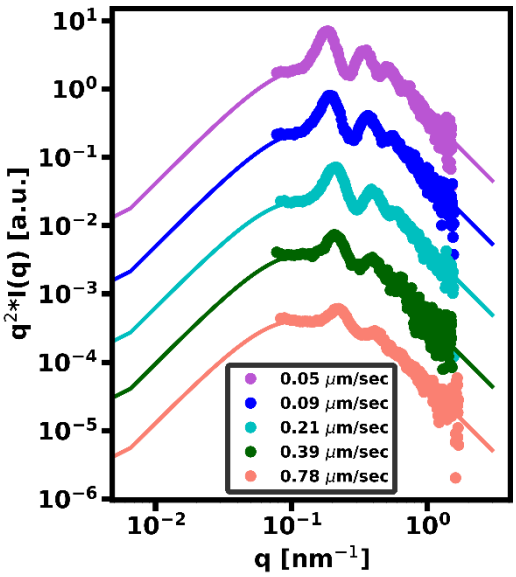

Figure S1. Extrapolation of scattering data for calculation of correlation function. Debye-Bueche is used for extrapolation to $q = 0$, while Porod's law for pinhole collimation is used for $q \to \infty$. Smooth lines are extrapolated data.

The extraction of the structural parameters from the correlation function is based on the self-correlation triangle for a perfect two-phase system.[12–14] The inherent disorder in semicrystalline polymers damps the oscillations; care must be

taken to interpret the parameters appropriately. The long period is the r-value corresponding to the first maximum of the correlation function, as this corresponds to the most probable value of L; these are plotted in Figure 3A in red.

The first intercept along the abscissa of the linear fit to the self-correlation portion of the correlation function is denoted as r_0; the linear crystallinity, w_c, is then calculated from $r_0 = w_c(1 - w_c)L$ for $w_c > 0.5$; the w_c values calculated in this manner for the zone annealed samples are plotted in Figure 3B as the red symbols. The baseline of the self-correlation triangle can also be extracted, though we do not use it here since derivation of structural parameters from the baseline assumes *a priori* that $w_c < 0.3$ or $w_c > 0.7$ and that the lamellar stacks are infinite.[13,14]

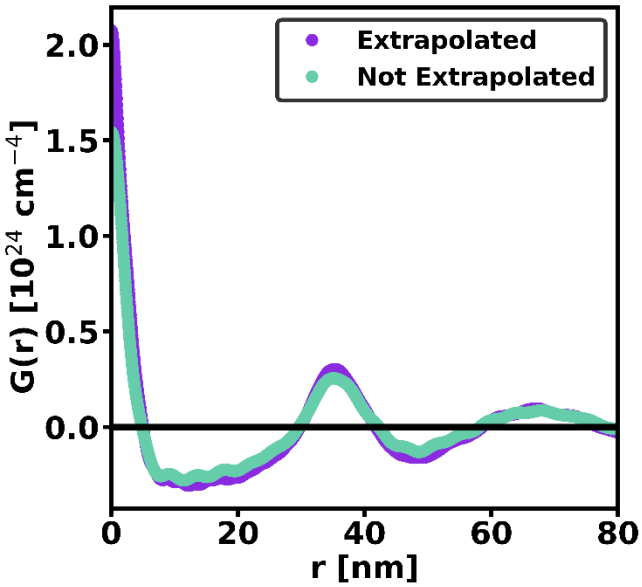

Figure S2. Calculation of correlation function with (purple) and without (green) extrapolation of $I(q)$ data to $q = 0$ and $q \to \infty$.

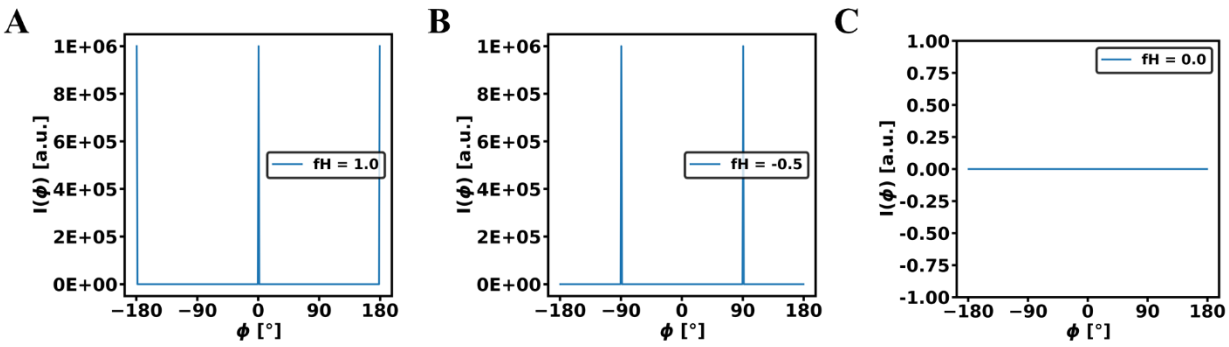

Figure S3. Calculation of Hermans orientation function for edge cases. (A) Delta function at $\phi = 0°, \phi = 180°, \phi = -180°$. (B) Delta function at $\phi = 90°, \phi = -90°$. (C) Flat intensity profile.

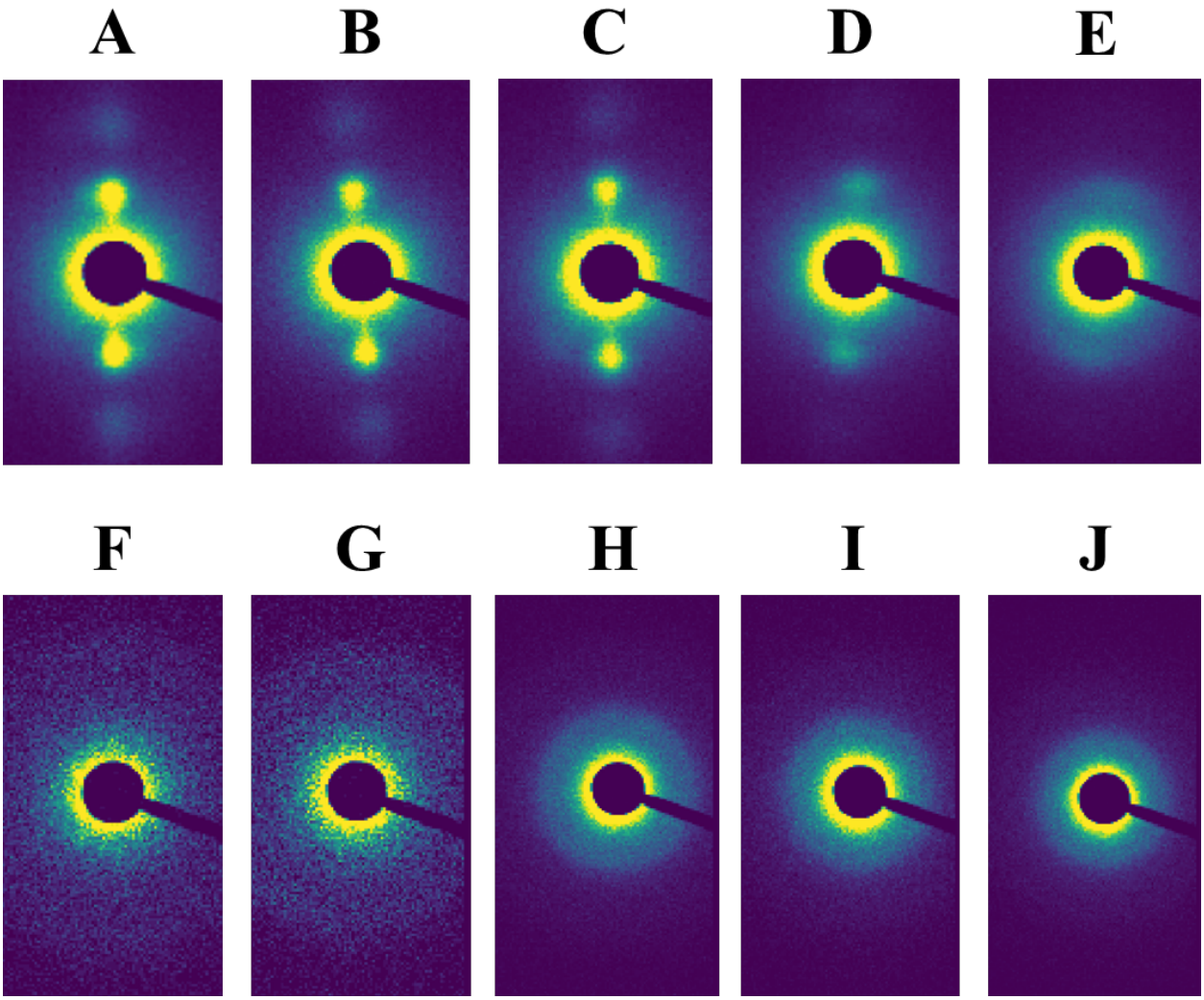

Figure S4. Representative 2D SAXS patterns of (top row) zone annealed and (bottom row) isothermally crystallized samples. (A) 0.05 μm/sec. (B) 0.09 μm/sec. (C) 0.21 μm/sec. (D) 0.39 μm/sec. (E) 0.78 μm/sec. (F) 52 °C. (G) 54 °C. (H) 56 °C. (I) 57 °C. (J) 58 °C.

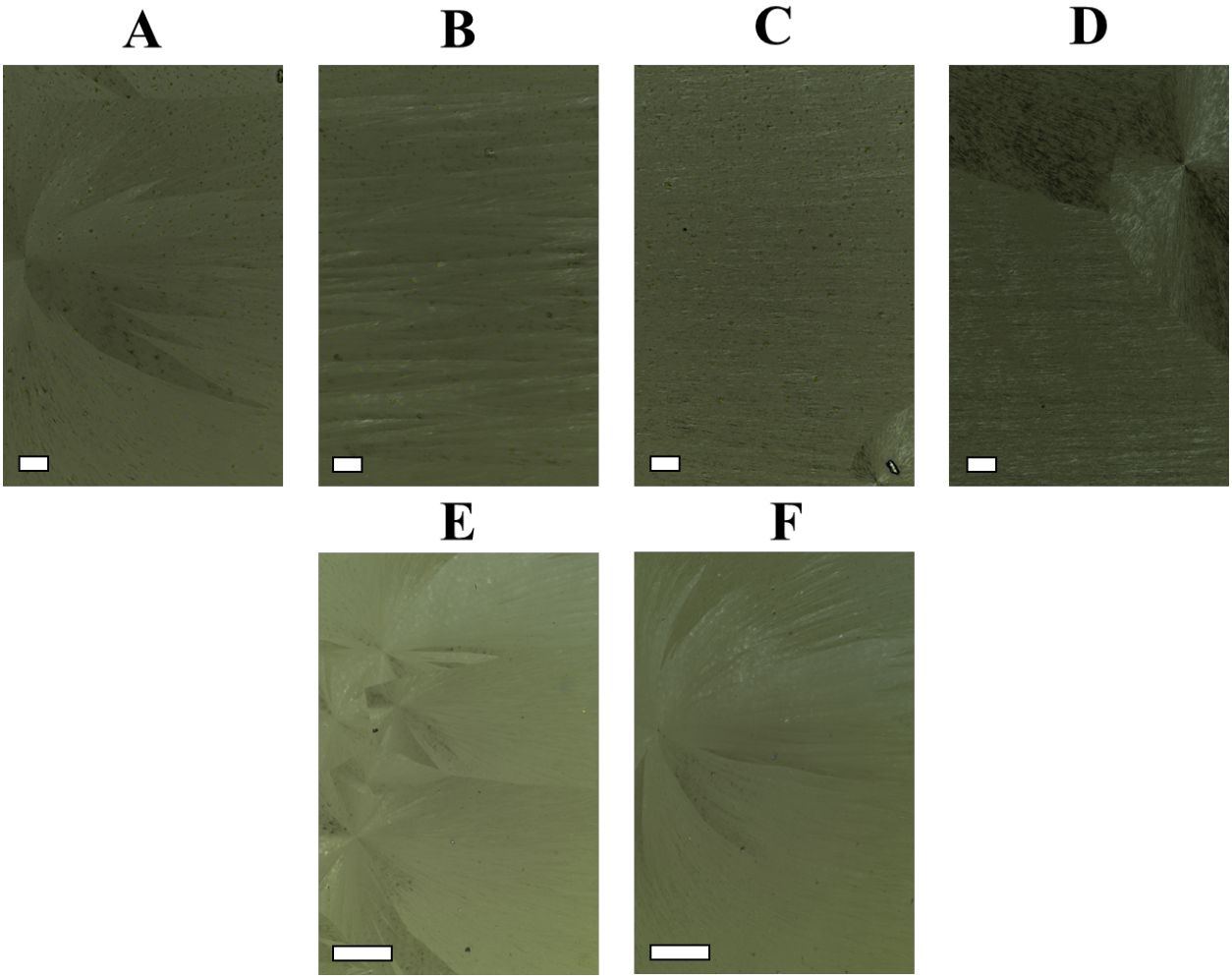

Figure S5. Additional polarized light optical microscopy images for a sample zone annealed at 0.39 μm/sec. Pulling direction is right to left (heat source direction is left to right). Scale bars are 100 μm and 500 μm for top and bottom rows, respectively. (A), (E), and (F) are near nucleation sites, while (B), (C), and (D) are further downstream.

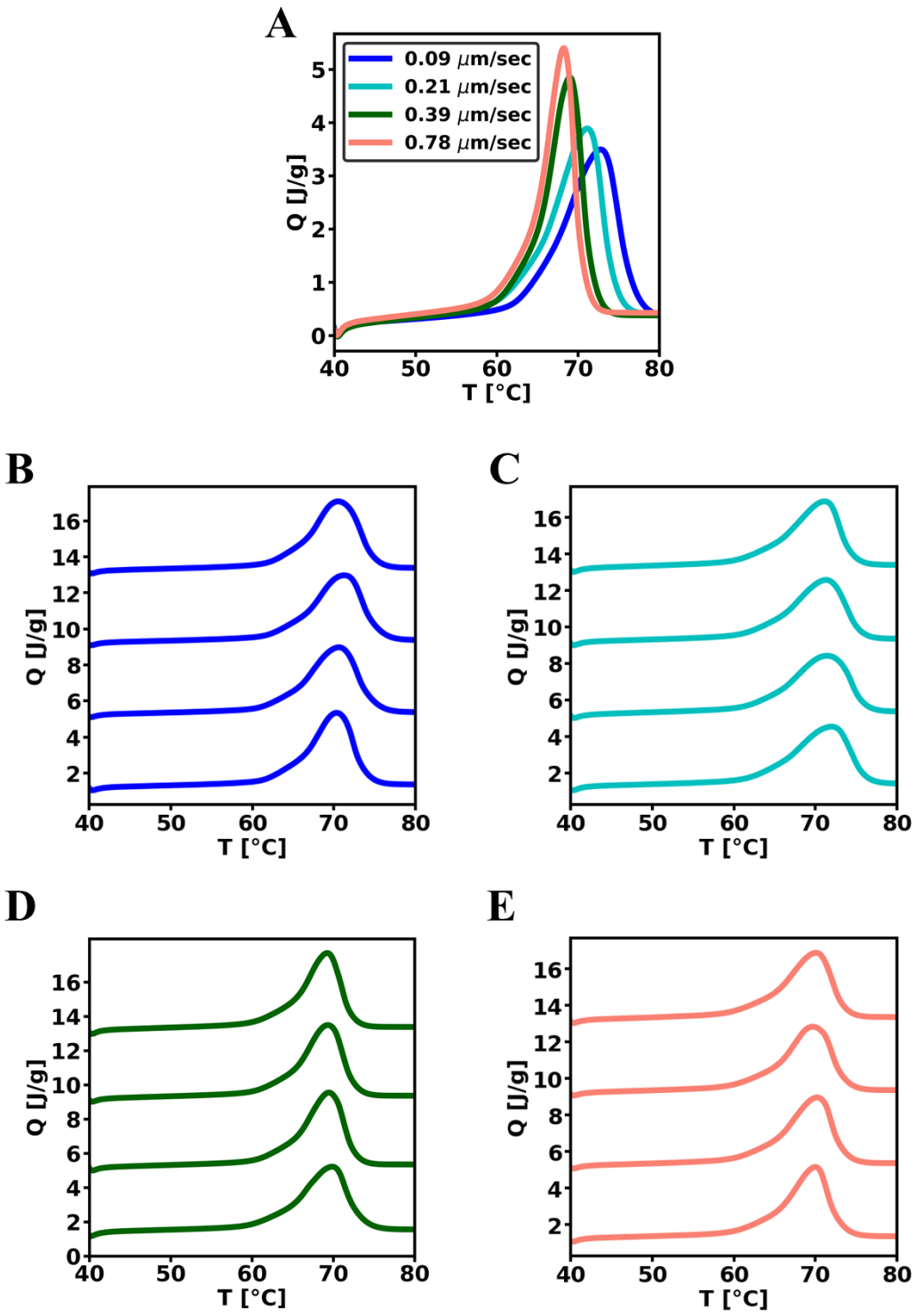

Figure S6. Representative DSC heat flow curves for zone annealed samples, taken from the first heating ramp at 10°C/min. (A) Compilation of representative curves for different velocities. Representative curves for (B) 0.09 μm/sec, (C) 0.21 μm/sec, (D) 0.39 μm/sec, and (E) 0.78 μm/sec.

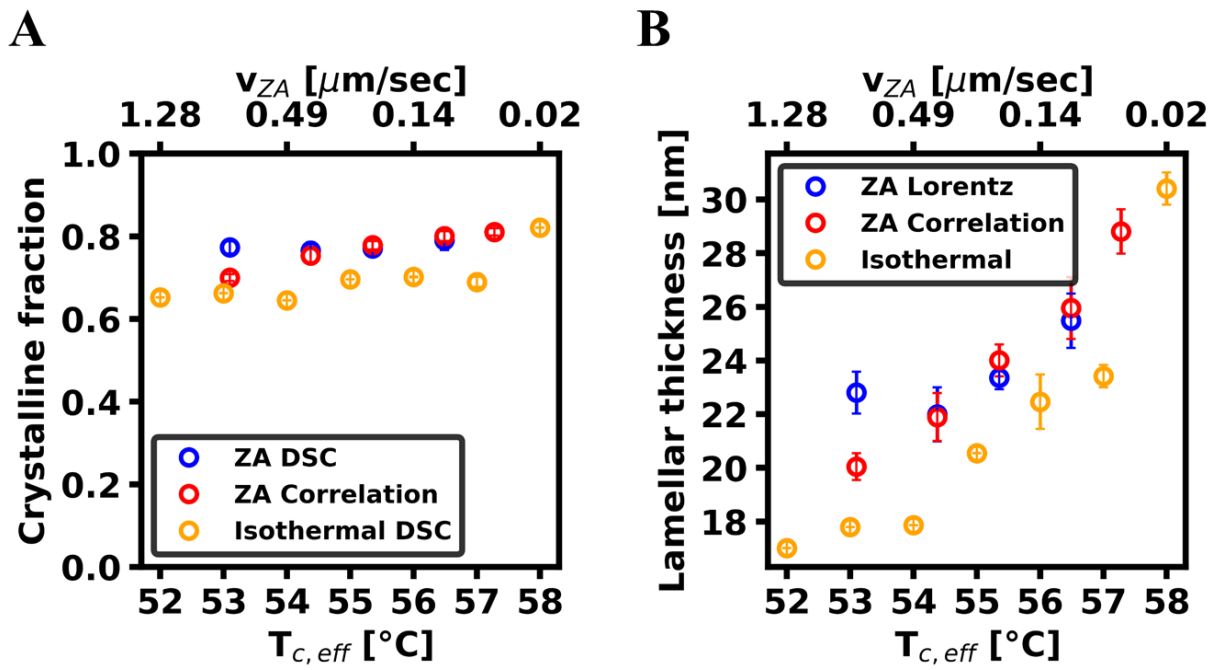

Figure S7. (A) Bulk crystalline volume fraction $\varphi_{c,v}$ from DSC for zone annealing (blue) and isothermal (orange), and linear crystallinity $w_c = \frac{1+\sqrt{1-\frac{4r_0}{L}}}{2}$ from the correlation function for zone annealing (red). (B) Lamellar thickness, calculated as $L * \varphi_{c,v}$ from the Lorentz-corrected profiles and DSC for zone annealing (blue) and isothermal (orange), and $L * w_c$ from the correlation function for zone annealing (red).

REFERENCES

(1) Jimenez, A. M.; Krauskopf, A. A.; Pérez-Camargo, R. A.; Zhao, D.; Pribyl, J.; Jestin, J.; Benicewicz, B. C.; Müller, A. J.; Kumar, S. K. Effects of Hairy Nanoparticles on Polymer Crystallization Kinetics. *Macromolecules* **2019**, *52*, 9186–9198. https://doi.org/10.1021/acs.macromol.9b01380.

(2) Ashiotis, G.; Deschildre, A.; Nawaz, Z.; Wright, J. P.; Karkoulis, D.; Emmanuel Picca, F.; Kieffer, J. The Fast Azimuthal Integration Python Library: PyFAI. *J. Appl. Crystallogr.* **2015**, *48* (2), 510–519. https://doi.org/10.1107/S1600576715004306.

(3) Mark, J. E. *Physical Properties of Polymers Handbook*; 2007.

(4) Lorenzo, A. T.; Arnal, M. L.; Albuerne, J.; Müller, A. J. DSC Isothermal Polymer Crystallization Kinetics Measurements and the Use of the Avrami Equation to Fit the Data: Guidelines to Avoid Common Problems. *Polym. Test.* **2007**, *26* (2), 222–231. https://doi.org/10.1016/j.polymertesting.2006.10.005.

(5) Wunderlich, B. *Macromolecular Physics*; 1973. https://doi.org/10.1016/B978-0-12-765601-4.50007-X.

(6) Zhu, L.; Cheng, S. Z. D.; Calhoun, B. H.; Ge, Q.; Quirk, R. P.; Thomas, E. L.; Hsiao, B. S.; Yeh, F.; Lotz, B. Phase Structures and Morphologies Determined by Self-Organization, Vitrification, and Crystallization: Confined Crystallization in an Ordered Lamellar Phase of PEO-b-PS Diblock Copolymer. *Polymer (Guildf).* **2001**, *42*, 5829–5839.

(7) Hoffman, J. D.; Miller, R. L. Kinetics of Crystallization from the Melt and Chain Folding in Polyethylene Fractions Revisited: Theory and Experiment. *Polymer (Guildf).* **1997**, *38* (13), 3151–3212. https://doi.org/10.1016/S0032-3861(97)00071-2.

(8) Chatterjee, T.; Lorenzo, A. T.; Krishnamoorti, R. Poly(Ethylene Oxide) Crystallization in Single Walled Carbon Nanotube Based Nanocomposites: Kinetics and Structural Consequences. *Polymer (Guildf).* **2011**, *52* (21), 4938–4946. https://doi.org/10.1016/j.polymer.2011.08.029.

(9) Laoutid, F.; Estrada, E.; Michell, R. M.; Bonnaud, L.; Müller, A. J.; Dubois, P. The Influence of Nanosilica on the Nucleation, Crystallization and Tensile Properties of PP-PC and PP-PA Blends. *Polymer (Guildf).* **2013**, *54* (15), 3982–3993. https://doi.org/10.1016/j.polymer.2013.05.031.

(10) Strobl, G. R.; Schneider, M. Direct Evaluation of the Electron Density Correlation Function of Partially Crystalline Polymers. *J. Polym. Sci. Polym. Phys. Ed.* **1980**, *18*, 1343–1359.

(11) Debye, P.; Bueche, A. M. Scattering by an Inhomogeneous Solid. *J. Appl. Phys.* **1949**, *20,* 518.

(12) Russell, T. P.; Ito, H.; Wignall, G. D. Neutron and X-Ray Scattering Studies on Semicrystalline Polymer Blends. *Macromolecules* **1988**, *21* (6), 1703–1709. https://doi.org/10.1021/ma00184a029.

(13) Talibuddin, S.; Wu, L.; Runt, J.; Lin, J. S. Microstructure of Melt-Miscible, Semicrystalline Polymer Blends. *Macromolecules* **1996**, *29* (23), 7527–7535. https://doi.org/10.1021/ma960508f.

(14) Fragiadakis, D.; Runt, J. Microstructure and Dynamics of Semicrystalline Poly(Ethylene Oxide)-Poly(Vinyl Acetate) Blends. *Macromolecules* **2010**, *43*, 1028–1034. https://doi.org/10.1021/ma9020938.